

Microscopic description of spontaneous fission based on a Gogny energy density functional including tensor contributions

R. Rodríguez-Guzmán,^{1,*} L. M. Robledo,^{2,3,†} and R. N. Bernard^{4,‡}

¹*Physics Department, Nazarbayev University, 53 Kabanbay Batyr Ave., Astana 010000, Kazakhstan*

²*Center for Computational Simulation, Universidad Politécnica de Madrid, Campus Montegancedo, 28660 Boadilla del Monte, Madrid, Spain*

³*Departamento de Física Teórica and CIAFF, Universidad Autónoma de Madrid, 28049-Madrid, Spain*

⁴*CEA, DES, IRESNE, DER, SPRC, LEPh, 13115 Saint-Paul-lès-Durance, France*

(Dated: October 18, 2024)

This paper extends previous studies on the impact of tensor forces in fission dynamics of neutron-deficient Thorium isotopes to other isotopic chains of heavy actinides and low-mass super-heavy nuclei. Calculations are carried out within a mean-field framework based on the Gogny-D1S parametrization supplemented with the D1ST2a perturbative tensor term as driving force. Fission barrier heights and spontaneous fission half-lives are used as benchmarks to analyze the impact of the tensor term. A significant reduction of fission barrier heights and half-lives is associated to the tensor component of the force.

PACS numbers: 24.75.+i, 25.85.Ca, 21.60.Jz, 27.90.+b, 21.10.Pc

I. INTRODUCTION

Nuclear fission is the consequence of large-amplitude collective motion driving the initial configuration (mostly the ground state of the parent nucleus) to scission point. Dynamics strongly depends on the nuclear interaction used as the associated (quantum) shell effects and pairing properties are responsible for tunneling through different stages of the evolution to scission. In addition, many-body methods used to (approximately) describe fission must be rooted in quantum mechanics for a sound microscopic description of the phenomenon. In spite of the many years passed since the experimental discovery of fission [1] and its initial interpretation [2, 3], the nuclear physics community has not reached a consensus on the optimal phenomenological interaction to be used to describe fission [4]. The consensus is necessary as the so-called *ab-initio* interactions inspired in the fundamental theory of strong interactions are still very far away to provide a consistent description of the phenomenon. There is also a vivid debate on the most suitable many-body method to be used to describe fission observables like spontaneous fission life-time or fission fragment mass distribution. Among the wide variety of approaches employed to describe fission [5], the constrained mean-field framework [6] has already been shown to represent a valuable tool, complementary to other theoretical models, to be used as zero order approximation to the problem.

Once the phenomenological interaction is chosen, fission is understood at the mean-field level in terms of a fission path parametrized as a function of the evolution of deformation parameters characterizing the different shapes involved. Associated to the fission path one

considers a potential energy, obtained at the mean-field level plus some corrections to be defined latter, with an associated complex landscape -comprising minima, valleys, ridges and saddle points consequence of shell effects. Given the importance of pairing, the potential energy is built using the Hartree-Fock-Bogoliubov (HFB) method with constrains on several deformation parameters denoted in the following as \mathbf{Q} [5, 7]. In addition to energies $E_{HFB}(\mathbf{Q})$, a microscopic description of fission requires collective inertias for the deformation degrees of freedom as well as the quantum zero-point vibrational $E_{VIB}(\mathbf{Q})$ corrections. The fission path involves strongly deformed configurations for which the rotational correction to the total energy $E_{ROT}(\mathbf{Q})$ is not a negligible quantity both because of its magnitude as well as its behavior as a function of \mathbf{Q} . All these ingredients define the collective potential $V(\mathbf{Q}) = E_{HFB}(\mathbf{Q}) - E_{VIB}(\mathbf{Q}) - E_{ROT}(\mathbf{Q})$ [7–10]. Both the collective inertias and the potential $V(\mathbf{Q})$, are employed to compute the spontaneous fission half-lives t_{SF} using the Wentzel-Kramers-Brillouin (WKB) approximation [7]. Those collective inertias and potential $V(\mathbf{Q})$ also represent basic ingredients within the Time Dependent Generator Coordinate Method (TDGCM) in the Gaussian Overlap Approximation (GOA), employed to extract observables such as the charge and/or mass distributions of the fission fragments [11–13].

Microscopic fission calculations are usually carried out using the least energy (LE) scheme. In this case, for a set of constrains \mathbf{Q} defining a configuration along the fission path, the HFB energy $E_{HFB}(\mathbf{Q})$ is minimized according to the Ritz-variational principle [6]. The quantum zero-point corrections are usually included *a posteriori* [7]. Among the assorted repertoire of phenomenological interactions, LE calculations are typically carried out in terms of nonrelativistic Gogny [7–10, 14–21], Skyrme [22–26] and Barcelona-Catania-Paris-Madrid (BCPM) [27–29] as well as relativistic [30–36] energy density functionals (EDFs).

* raynerrobertorodriguez@gmail.com

† luis.robledo@uam.es

‡ remi.bernard@cea.fr

A second class of calculations -which have already received close scrutiny using both non-relativistic and relativistic approaches- resorts to the least action (LA) scheme. Here, the quantum zero-point corrections are also included *a posteriori* [37]. A key result, emerging from previous LA studies, is that the collective action gets strongly quenched when pairing degrees of freedom are included, leading to a substantial decrease of several orders of magnitude in the computed t_{SF} values. As a consequence, a much better agreement with the available experimental data [37–45] is obtained in comparison with LE calculations.

Regardless of the LE and/or LA scheme considered, an implicit assumption in microscopic fission calculations is that, fission-related properties are determined by general features of the effective interactions employed. However, interactions are usually tuned to reproduce nuclear matter parameters -such as the surface energy of semi-infinite nuclear matter- that are not properly constrained by experimental data and it is important to include fission data in their fitting protocol as done in Refs. [14, 22, 46–48].

In the case of the Gogny-EDF, the parametrization D1S was introduced to reduce the too large fission barrier height obtained with the previous parametrization and subsequently applied to the microscopic description of fission in heavy and superheavy nuclei [15, 18, 19]. This parametrization, considered a well tested standard within the Gogny-D1 family, has shown its ability to reproduce reasonably well several other properties all over the nuclear chart both at the mean-field level and beyond [47]. Nevertheless, it has also been found that the Gogny-D1S EDF is not specially good in reproducing masses when moving away from the stability valley. To cure this deficiency, new parametrizations -such as D1N [49] and D1M [50]- have been introduced in the Gogny-D1 family. Previous studies have already shown that, while improving the description of nuclear masses, D1M essentially retains the same predictive power as D1S to account for fission properties in heavy and superheavy nuclei [7–10, 20, 21, 37, 40] as well as for a wealth of low-energy nuclear structure data [47, 51–58].

In spite of their reasonable performance, none of the members of the Gogny-D1 family already mentioned include a tensor force. Such tensor components have received attention in Skyrme mean-field calculations for both spherical and deformed nuclei [59, 60]. In the case of the Gogny-EDF, like-particle tensor components were first considered to improve the evolution of spherical single-particle states along isotopic chains, but no attention was paid to pairing correlations [61]. Later, a complete long range tensor has been added perturbatively to the standard Gogny-D1S EDF [62–66]. The reshuffling of single particle orbitals around the Fermi level brought about by the tensor interaction can have a sizable impact both on the amount of shell effects responsible for barrier properties as well as in the strength of pairing correlations crucial to determine collective inertias.

Previous studies [67–69] have shown that second-order

tensor corrections mostly affect the ($S = 1, T = 0$) channel and, in the fitting protocol of the original Gogny-EDF, most of the effect of the tensor force was already phenomenologically included in the strength of the density-dependent term, which also acts in the ($S = 1, T = 0$) channel. Therefore, the inclusion of a perturbative long range tensor in the parametrization D1ST2a (to be referred simply as D1ST hereafter) [62–66] represents a meaningful first step towards a full refitting of all the parameters of the Gogny-EDF.

Much work still remains to be done to assess the impact of a tensor term like the one in Gogny-D1ST in the microscopic description of fission properties in heavy and superheavy nuclei. The first exploration of the role of tensor contributions in fission properties was carried out on a fission calculation for a selected set of neutron deficient Th isotopes [70] for which recent experimental data has been obtained [71] in the SOFIA collaboration [72]. It is found, that tensor contributions are crucial for the opening a new valley, associated with the exotic symmetric bimodal fission observed in those neutron-deficient Th isotopes [71, 73].

To the best of our knowledge, a survey of spontaneous fission half-lives and related properties, using the Gogny-D1ST EDF, has not yet been presented in the literature. This is precisely, the goal of this mean-field study using the LE scheme. By using the D1ST parametrization along with the HFB approximation [6] calculations for the isotopic chains $^{240-250}\text{Cm}$ and $^{240-250}\text{Cf}$, for which experimental data are available [74], are carried out and the outcome compared with results obtained with the standard D1S parametrization. Comparison of the predicted lifetimes and other properties, obtained with both EDFs, represents a timely and necessary step to better understand the role of tensor contributions in the fission properties of those isotopes belonging to a region of the nuclear chart where several key features of the shell effects associated with superheavy elements start to manifest [7, 8, 20, 37]. Moreover, we have extended the calculations to the low-Z superheavy nuclei $^{242-258}\text{Fm}$. Such a chain, with a belt-shaped dependence of the spontaneous fission half-lives as functions of the mass number [74], represents a challenging benchmark to further examine the fission properties associated to the Gogny-D1ST EDF.

The paper is organized as follows. In Sec. II, we briefly outline the theoretical LE framework employed to study the fission properties of the considered nuclei. The results of our calculations are discussed in Sec. III. We start the section, with a description of our D1S and D1ST Gogny-HFB calculations for the nucleus ^{248}Cf taken as an illustrative example. The same methodology has been employed for all the considered nuclei. Next, we present the D1S and D1ST systematic of the fission paths and spontaneous fission half-lives for the studied Curium and Californium isotopes. The section ends, with a discussion of the D1S and D1ST systematic of the spontaneous fission half-lives obtained for $^{242-258}\text{Fm}$. In Sec. III, we also

compare with the available experimental t_{SF} values [74]. Finally, Sec. IV is devoted to the concluding remarks.

II. THEORETICAL FRAMEWORK

The results discussed in this paper, have been obtained with the standard D1S [14] and D1ST [62–66] parametrization of the Gogny-EDF. The effective two-body D1ST force reads

$$V(\vec{r})_{\text{D1ST}} = \sum_{i=1,2} \left(W_i + B_i P_{12}^\sigma + H_i P_{12}^\tau + W_i P_{12}^\sigma P_{12}^\tau \right) e^{-\frac{\vec{r}^2}{\mu_i^2}} \text{ where the action } S \text{ along the (one-dimensional } Q_{20}\text{-projected) fission path reads}$$

$$+ t_0 \left(1 + x_0 P_{12}^\sigma \right) \rho^\alpha(\vec{R}) \delta(\vec{r})$$

$$+ W_{LS} \overleftarrow{\nabla} \delta(\vec{r}) \wedge \overrightarrow{\nabla} \cdot \left(\vec{\sigma}_1 \cdot \vec{\sigma}_2 \right)$$

$$+ \left(V_{T1} + V_{T2} P_{12}^\tau \right) S_{12}(\vec{r}) e^{-\frac{\vec{r}^2}{\mu_{TS}^2}}$$

$$(1) \quad S(Q_{20}) = \sqrt{2B(Q_{20}) \left(V(Q_{20}) - (E_{Min} + E_0) \right)} \quad (5)$$

where

$$S_{12}(\vec{r}) = 3 \frac{(\vec{\sigma}_1 \cdot \vec{r})(\vec{\sigma}_2 \cdot \vec{r})}{r^2} - \vec{\sigma}_1 \cdot \vec{\sigma}_2 \quad (2)$$

In this expression \vec{r} and \vec{R} stand for the relative and center of mass coordinate of two particles.

The first three lines in Eq.(1) correspond to any standard member of the Gogny-D1 family, the only differences being in the values of the parameters. In the case of the effective D1ST force, the values of the parameters $\{W_i, B_i, H_i, M_i, \mu_i, i = 1, 2\}$, t_0 , x_0 , α and W_{LS} are the same as the ones in the standard Gogny-D1S force [14]. On the other hand, the tensor parameters V_{T1} and V_{T2} have been adjusted to reproduce the $1f_{5/2}$ and $1f_{7/2}$ neutron single-particle energies in ^{48}Ca . The range of the spatial form factor is taken equal to the largest range of the central potential of D1S, namely $\mu_{TS} = 1.2$ fm.

Axial and simplex symmetries have been kept as self-consistent symmetries [6]. In addition to the usual HFB constrains on the proton and neutron number operators [6], we have employed constrains on the quadrupole $\hat{Q}_{20} = z^2 - \frac{1}{2}(x^2 + y^2)z$ and octupole $\hat{Q}_{30} = z^3 - \frac{3}{2}(x^2 + y^2)z$ operators [37, 51, 54] to obtain the D1S and/or D1ST deformation properties.

The quasiparticle operators [6] have been expanded in a deformed axially symmetric harmonic oscillator (HO) basis containing states with J_z quantum numbers up to $35/2$ and up to 26 quanta in the z-direction. For each of the configurations along the fission paths of the studied nuclei, the HO lengths b_\perp and b_z have been optimized so as to minimize the total HFB energy.

For the solution of the HFB equations, an approximate second order gradient method [75] has been used. The two-body kinetic energy correction has been fully taken into account in the Ritz-variational [6] procedure. In the calculations, Coulomb exchange is evaluated in

the Slater approximation [76] while Coulomb and spin-orbit antipairing are neglected. As in previous works [62–66, 70], the tensor contribution is only included in the Hartree-Fock field while its contribution to the pairing field is neglected. Preliminary results seem to indicate that the tensor pairing field is small as compared to other contributions and has little impact on fission dynamics.

We have computed the spontaneous fission half-lives t_{SF} (in seconds) using the WKB formalism

$$t_{SF} = 2.86 \times 10^{-21} \times (1 + e^{2S}) \quad (3)$$

$$S = \int_a^b dQ_{20} S(Q_{20}) \quad (4)$$

with the integrand

$$S(Q_{20}) = \sqrt{2B(Q_{20}) \left(V(Q_{20}) - (E_{Min} + E_0) \right)} \quad (5)$$

The integration limits a and b in Eq.(4) correspond to classical turning points [77] evaluated for the energy $E_{Min} + E_0$. The energy E_{Min} corresponds to the absolute minimum of the considered path, while E_0 accounts for the true ground state energy once quadrupole fluctuations are taken into account. This quantity can be estimated with a harmonic approximation using the curvature of the potential around the minimum and the collective inertia of the quadrupole motion. Typical values obtained in the region are around 0.5 MeV with some fluctuations associated to variations with neutron number. In order to better disentangle the effect of the tensor term a constant value $E_0 = 0.5$ MeV has been employed in this work.

In Eq.(5), $B(Q_{20})$ represents the quadrupole collective mass, while the collective potential $V(Q_{20})$ reads [7–10]

$$V(Q_{20}) = E_{HFB}(Q_{20}) - E_{VIB}(Q_{20}) - E_{ROT}(Q_{20}) \quad (6)$$

with $E_{HFB}(Q_{20})$, $E_{VIB}(Q_{20})$ and $E_{ROT}(Q_{20})$ being the HFB, vibrational and rotational correction energies, respectively, as functions of the quadrupole deformation Q_{20} .

The collective mass $B(Q_{20})$ as well as the zero-point vibrational energy $E_{VIB}(Q_{20})$ have been computed using the perturbative cranking approximation [7, 78–80] to the Adiabatic Time Dependent HFB (ATDHFB) and the Gaussian Overlap Approximation (GOA) [6, 7]. The zero-point rotational energy $E_{ROT}(Q_{20})$ has been computed in terms of the Yoccoz moment of inertia [81–83]. Therefore, in this study two different paths -the GCM and the ATDHFB paths- will be considered for each nucleus with the D1S and D1ST EDFs.

III. DISCUSSION OF THE RESULTS

In this section, the results obtained for the $^{240-250}\text{Cm}$, $^{240-250}\text{Cf}$ and $^{242-258}\text{Fm}$ isotopic chains are discussed.

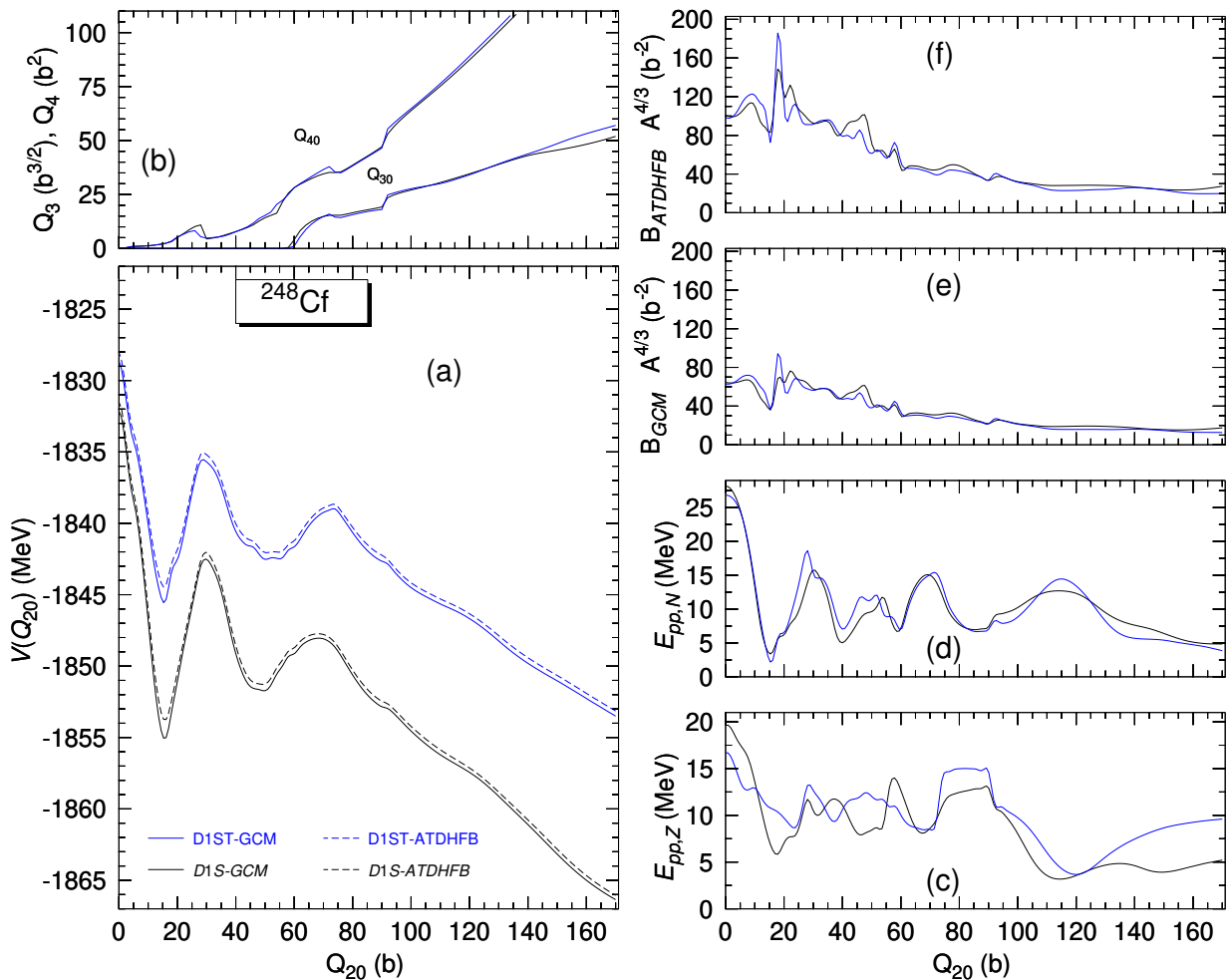


FIG. 1. (Color online) The collective potentials $V(Q_{20})$ Eq.(6) obtained for the nucleus ^{248}Cf , within the GCM and ATDHFB schemes, are plotted in panel (a) as functions of the quadrupole moment Q_{20} . The octupole Q_{30} and hexadecapole Q_{40} moments of the intrinsic states are plotted in panel (b). The proton $E_{pp,Z}$ and neutron $E_{pp,N}$ pairing interaction energies are depicted in panels (c) and (d), while the collective GCM and ATDHFB masses are plotted in panels (e) and (f). Results have been obtained with the parametrizations D1S and D1ST of the Gogny-EDF. For more details, see the main text.

Let us first describe in more detail the results obtained for the nucleus ^{248}Cf , taken as an illustrative example. The GCM and ATDHFB collective potentials $V(Q_{20})$ Eq.(6), obtained for this nucleus, are plotted in panel (a) of Fig. 1 as functions of the quadrupole moment Q_{20} of the intrinsic states.

The first noticeable feature, is the underbinding of the D1ST curves with respect to the D1S ones. For example, for $Q_{20} = 16$ b, $\delta V_{GCM} = V_{GCM}^{D1ST} - V_{GCM}^{D1S} = 9.64$ MeV and $\delta V_{ATDHFB} = V_{ATDHFB}^{D1ST} - V_{ATDHFB}^{D1S} = 9.39$ MeV, respectively. Such a global underbinding of the D1ST HFB solutions -arising from the proton-neutron part of the tensor term- is a common feature for all the nuclei studied in this work and is a consequence of the features of the tensor term considered. Nevertheless, it is satisfying to observe that all the curves in panel (a) look rather similar with the ground state located at $Q_{20} = 16$ b and a fission isomeric state at $Q_{20} = 50$ b. However, although

the fission paths look quantitatively the same they differ in their barrier height. For D1S the top of the inner barrier is located around $Q_{20} = 30$ b, and its height reaches the values $B_{I,GCM} = 12.55$ MeV, $B_{I,ATDHFB} = 11.74$ MeV whereas for D1ST one obtains $B_{I,GCM} = 9.79$ MeV and $B_{I,ATDHFB} = 9.20$ MeV, respectively, which are significantly lower than the D1S results. One has to keep in mind that triaxiality is not allowed in the calculation, a restriction that increases the barrier heights by one or two MeV. This effect cannot be included at the present stage along with the tensor force.

The reflection-symmetric fission isomer corresponding to the second excited minimum is located at $Q_{20} = 52$ b in the D1S case while it is shifted to a slightly larger quadrupole moment when the tensor interaction is considered. Excitation energies are $E_{II,GCM}^{D1S} = 3.34$ MeV, $E_{II,ATDHFB}^{D1S} = 2.52$ MeV, $E_{II,GCM}^{D1ST} = 2.90$ MeV and

$E_{II,ATDHFB}^{D1ST} = 2.34$ MeV. The effect of the tensor is to slightly reduce the fission isomer excitation energy but the effect is, by no means, relevant for fission dynamics. Regardless of the Gogny-EDF employed, octupole correlations play a prominent role in the outer sectors of the GCM and ATDHFB paths and are responsible for the asymmetric fission fragment mass distribution observed experimentally. In addition, octupole correlations significantly reduce the height B_{II} of the outer fission barrier. The position of the second barriers is predicted at 70 b (D1S) and 76 b (D1ST). The height of the second barrier obtained with D1S are $B_{II,GCM} = 7.01$ MeV and $B_{II,ATDHFB} = 6.04$ MeV, whereas slightly lower values are obtained for D1ST $B_{II,GCM} = 6.43$ MeV and $B_{II,ATDHFB} = 5.70$ MeV.

One can summarize the previous discussion by saying that the main effect of the tensor interaction is to reduce significantly the first barrier height. It is also responsible for a slight displacement of the position of the two minima, and the second barrier to larger values of the quadrupole moment. Finally, excitation energies of the fission isomer as well as second barrier heights are not modified in a substantial way. These effects are also visible in other isotopes, as it will be discussed below.

The octupole Q_{30} and hexadecupole Q_{40} moments of the intrinsic states are plotted in panel (b) of Fig. 1. As the spatial reflection symmetry can be broken at any stage of the calculations an additional constrain on the center of mass operator \hat{Q}_{10} has to be imposed to keep the center of mass fixed at the origin [37, 51, 54] to avoid spurious center of mass motion. As can be seen from the panel, the D1S and D1ST Q_{30} and Q_{40} values are rather similar. Note also from the panel, that for ^{248}Cf octupole deformations play a role for $Q_{20} \geq 56\text{-}58$ b roughly after the fission isomer minimum.

The proton and neutron pairing interaction energies $E_{pp,\tau} = \frac{1}{2}\text{Tr}(\Delta_\tau \kappa_\tau)$ (with $\tau = Z, N$) of the intrinsic states are plotted in panels (c) and (d). In the present case, only the Gaussian central potential contributes to these quantities. Therefore, the different pairing content in both functionals reflects the tensor rearrangement of the underlying single-particle spectra. As can be seen from panels (c) and (d), though some differences are also observed for the neutron-neutron pairing interaction energies, the most prominent differences are obtained for the proton-proton ones.

The collective GCM and ATDHFB masses $B(Q_{20})$ are depicted in panels (e) and (f). As already mentioned, those masses have been computed using the cranking approximation, and a three point filter has been employed to soften the wiggles associated to level crossings [7]. For $Q_{20} \leq 20$ b the D1ST masses are slightly larger than the D1S ones while for larger quadrupole moments the former are, on the average, smaller than the latter. Regardless of the considered Gogny-EDF, both the GCM and ATDHFB masses display a similar qualitative and quantitative trend. Such a trend is well correlated with the patterns observed in the pairing interaction energies

in panels (c) and (d), and reflects the inverse dependence of the collective masses with the square of the pairing gap [77, 84]. As mentioned before, the contribution of the tensor interaction to the pairing channel has been neglected. Given the strong dependence of the inertias with pairing correlations the pairing associated to the tensor term should be studied in depth in the future. Another feature that emerges is that both the D1S and D1ST ATDHFB masses are always larger than their GCM counterparts. This is the reason to include both kinds of collective masses in this study, as their differences can affect the predicted lifetimes by several orders of magnitude [7, 8]. In the case of ^{248}Cf and $E_0 = 0.5$ MeV, we have obtained the D1S (D1ST) GCM and ATDHFB values $\log_{10} t_{SF,GCM}^{D1S} = 15.66$ ($\log_{10} t_{SF,GCM}^{D1ST} = 12.71$) and $\log_{10} t_{SF,ATDHFB}^{D1S} = 20.06$ ($\log_{10} t_{SF,ATDHFB}^{D1ST} = 17.29$). The larger ATDHFB values are associated to the larger inertia that implies a larger action integral. These results should be compared with the corresponding experimental value $\log_{10} t_{SF} = 12$ [74].

The GCM and ATDHFB collective potentials $V(Q_{20})$, obtained for $^{240-250}\text{Cm}$ and $^{240-250}\text{Cf}$ are plotted in panels (a) to (f) of Figs. 2 and 3, as functions of Q_{20} . All the relative energies are measured with respect to the absolute minima of the corresponding paths to facilitate the comparisons. Let us remark, however, that for all the considered nuclei there is a global underbinding of the D1ST HFB solutions -arising from the proton-neutron part of the tensor term- with respect to the D1S solutions. In panel (e) of Fig. 3, results for ^{248}Cf are included for the sake of completeness. The excitation energies of the spherical configurations predicted with the Gogny-D1ST EDF are always smaller than the corresponding D1S values. For example, within the GCM scheme, the D1ST spherical configuration in ^{244}Cm (^{244}Cf) is predicted 6.91 (6.56) MeV below the D1S one. For the ATDHFB case, the values are very similar to the GCM ones, namely 6.64 (6.28) MeV.

The absolute minima of the collective potentials correspond to $Q_{20} = 14\text{-}16$ b. Inner and outer barriers, as well as reflection-symmetric fission isomers in between them, are apparent from Figs. 2 and 3. As can be seen from the figures, smaller barrier heights are obtained with the Gogny-D1ST EDF. However, the outer sectors of the fission path obtained with this EDF for Cm isotopes, exhibit a much gentler decline than the ones obtained with the standard D1S parametrization. This means that the tensor contribution is somehow affecting the surface tension coefficient of the interaction. However, it has to be determined whether a full refit of the force including the tensor term will reabsorb this effect into other components of the force. On the other hand, such an effect is less pronounced for Cf nuclei and therefore it is dependent on mass number.

The summit of the inner barriers is located at $Q_{20} = 26\text{-}30$ b. Regardless of the GCM and/or ADTHFB scheme employed, the heights B_I of the inner barriers in Cm (Cf) isotopes increase as functions of the mass

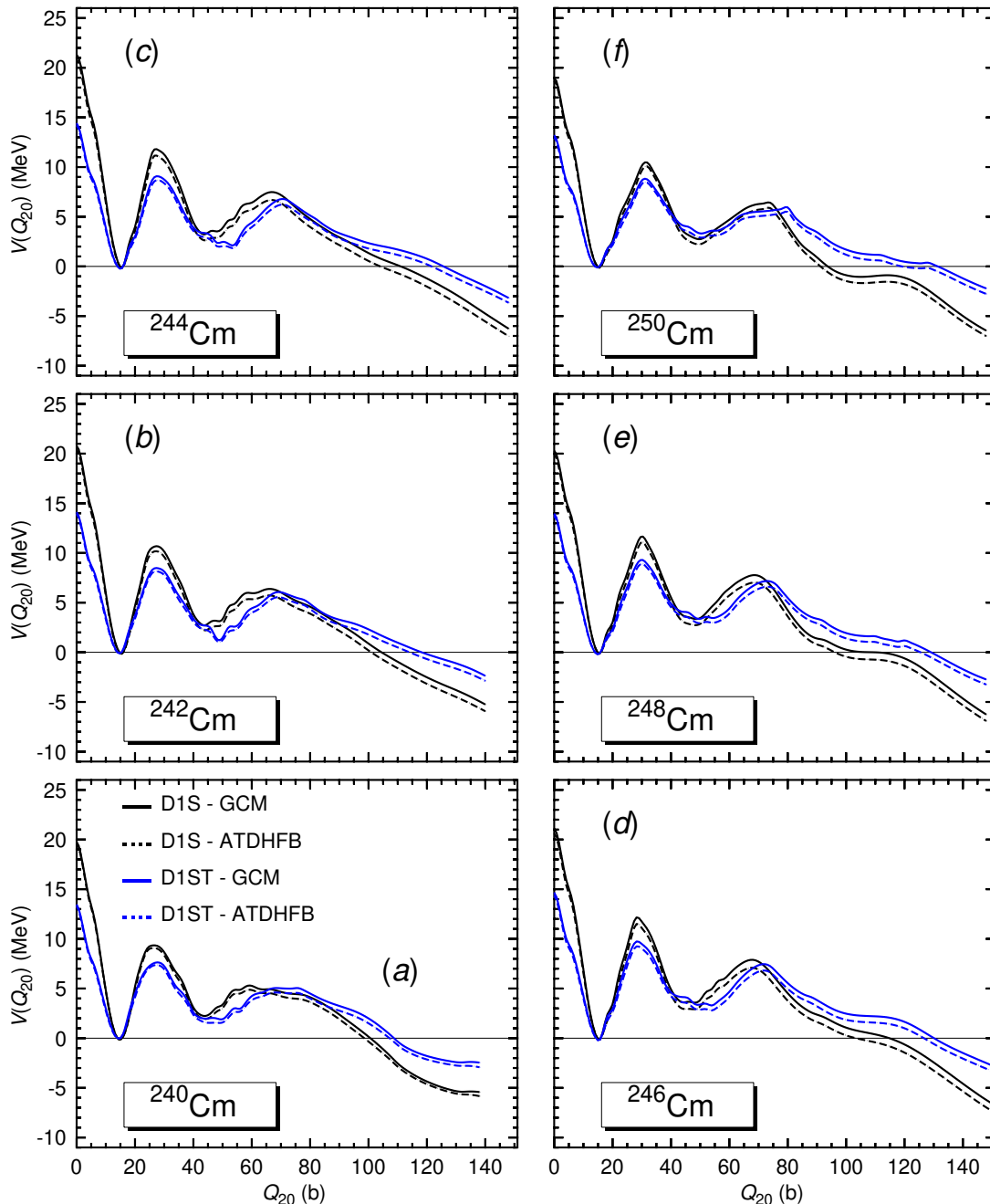


FIG. 2. (Color online) The collective potentials $V(Q_{20})$ Eq.(6) obtained for the nuclei $^{240-250}\text{Cm}$, within the GCM and ATDHFB schemes, are plotted as functions of the quadrupole moment Q_{20} . All the relative energies are measured with respect to the absolute minima of the corresponding paths. Results have been obtained with the parametrizations D1S and D1ST of the Gogny-EDF. For more details, see the main text.

number, reaching a maximum at $A = 246$ (248). As can be seen from the figures, the B_{II} values obtained with the parametrization D1ST are smaller than the D1S heights.

In the case of the outer barriers, their summit is located around $Q_{20} = 60-74$ b and $Q_{20} = 70-78$ b for the Cm and Cf isotopes, respectively. The outer barriers for $^{240,242}\text{Cf}$, display a two-humped structure with the summit located around $Q_{20} = 56$ b. The summit of the

outer barriers is located at slightly larger values of the quadrupole moment in calculations carried out with the Gogny-D1ST EDF. For the nuclei shown in Figs. 2 and 3, octupole correlations play a role for $Q_{20} \geq 54$ b, and affect the height B_{II} of the outer barriers significantly. Similar to the inner barriers, the heights B_{II} increase as functions of the mass number, reaching a maximum at $A = 246$ (248).

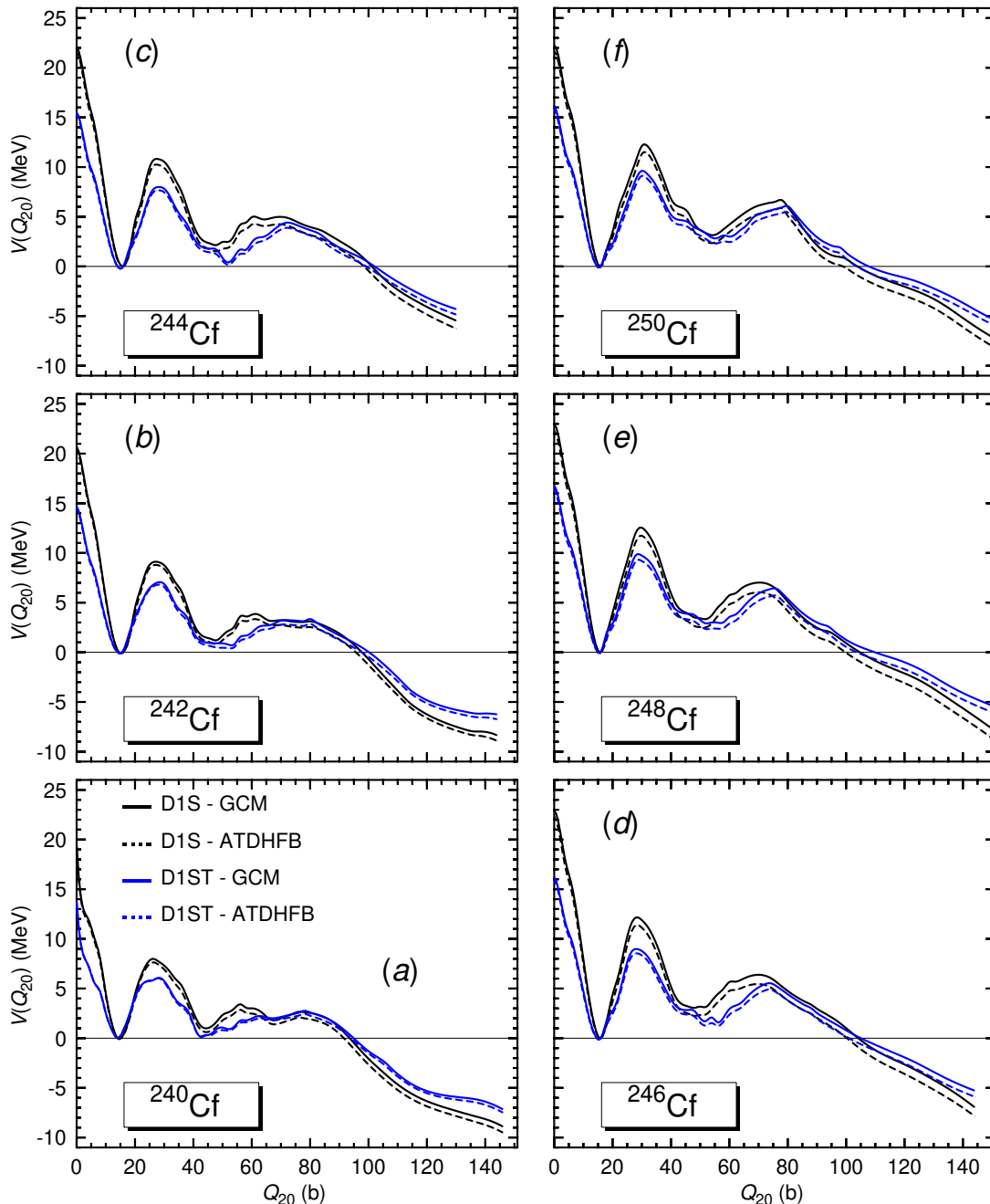


FIG. 3. (Color online) The same as Fig. 2 but for the nuclei $^{240-250}\text{Cf}$.

In the calculations, the smallest B_I and B_{II} heights are always predicted within the ATDHFB scheme and with the Gogny-D1ST EDF. Even when tensor correlations tend to reduced the heights of the inner barriers, the comparison (without triaxiality included) with the available experimental B_I^{exp} values for $^{242-248}\text{Cm}$ still reveals differences of 1.46, 2.51, 3.21 and 3.41 MeV. For $^{242-248}\text{Cm}$ and ^{250}Cf the differences between the predicted and experimental B_{II}^{exp} values are still 0.52, 1.11, 2.01, 1.77 MeV and 1.95 MeV, respectively [85, 86]. The Slater approximation to Coulomb exchange probably plays a role as

well here: it was shown that the impact of this approximation amounts to up to 1 MeV in the Thorium chain [70].

The previous results suggest that correlations not explicitly taken into account in this work might be required to improve the agreement with the available experimental data for (static) inner and outer barrier heights. For example, previous calculations without tensor correlations [7], based on the Gogny-D1M EDF, have found that for $^{242-248}\text{Cm}$ triaxiality reduces the predicted inner barrier height by 1.47, 2.11, 2.72 and 3.18 MeV. At this point,

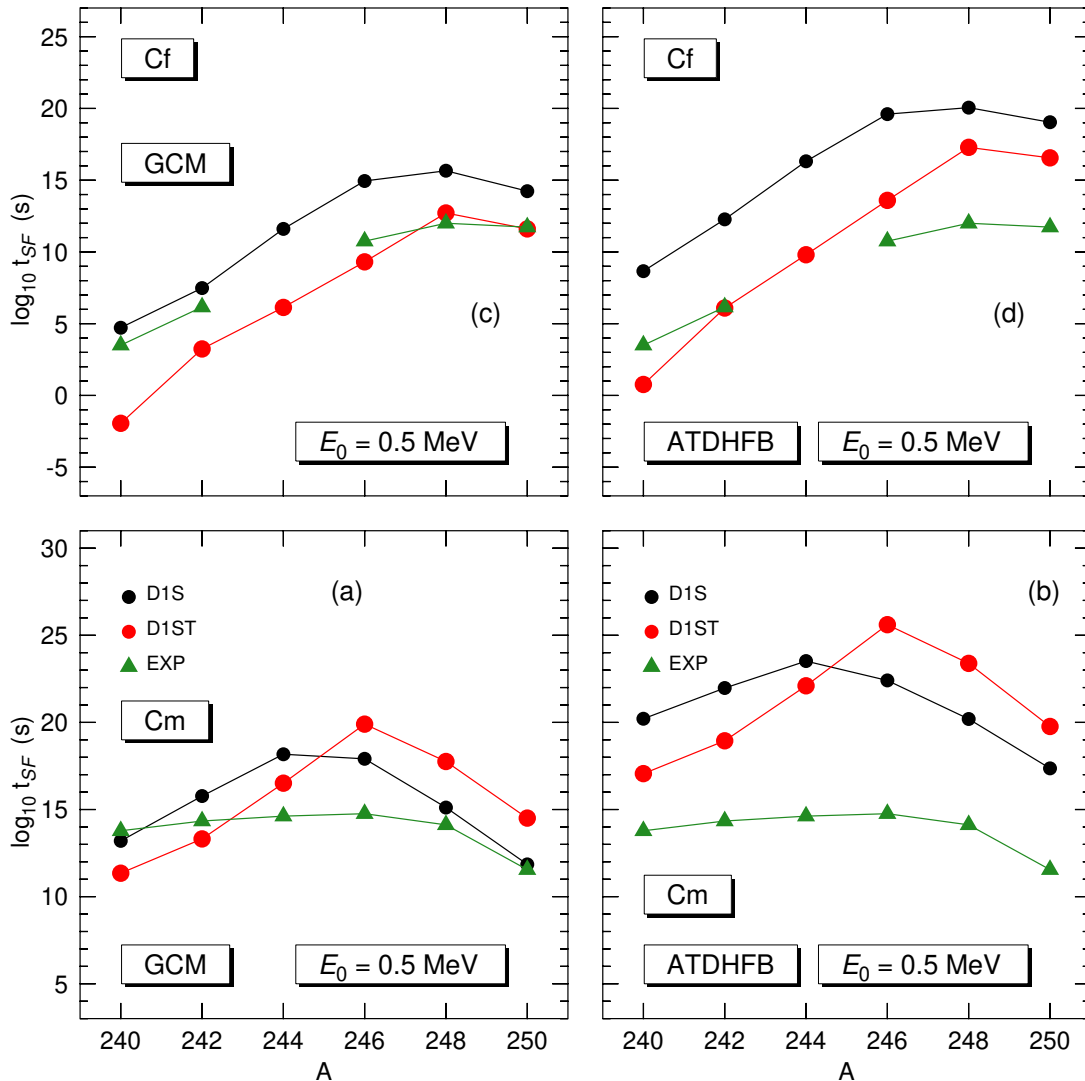


FIG. 4. (Color online) The spontaneous fission half-lives t_{SF} , predicted for the nuclei $^{240-250}\text{Cm}$ [$^{240-250}\text{Cf}$], within the GCM and ATDHFB schemes, are depicted in panels (a) and (b) [panels (c) and (d)] as functions of the mass number. Results have been obtained with the parametrizations D1S and D1ST of the Gogny-EDF and $E_0 = 0.5 \text{ MeV}$. The available experimental values, taken from Ref. [74], are included in the plots.

it is worth to remark that the heights of (static) fission barriers are not physical observables. Their values are inferred from the behavior of fission cross sections as a function of the energy and using certain model assumptions [87]. Moreover, for a given nucleus the spontaneous fission half-life Eq. (3) also depends on the shape and width of the barrier and, more generally, via Eqs. (4) and (5), on the topography of the collective potential in between the classical turning points as well as on the collective inertias.

A key lesson extracted from previous studies is that, caution must be taken in linking barrier heights with t_{SF} values [37, 39, 40]. As can be seen from Eq. (5), not only the collective potential but also the collective mass -with its implicit pairing dependence- does play a role in the predicted lifetime. Previous LA studies -in which,

the collective action is minimized with respect to pairing degrees of freedom- have shown that larger barrier heights do not necessarily translate into larger t_{SF} values [37, 39, 40]. In fact, it is the subtle interplay between the collective potential and the collective mass what leads to the final value for the spontaneous fission half-life. Note also, that pairing fluctuations within the LA scheme can restore axial symmetry along the fission path [43, 44] suggesting that the impact of triaxiality in the predicted lifetimes is quite limited.

Let us now turn our attention to the spontaneous fission half-lives predicted for the nuclei $^{240-250}\text{Cm}$ and $^{240-250}\text{Cf}$ with the parametrizations D1S and D1ST of the Gogny-EDF. For $^{240-250}\text{Cm}$ [$^{240-250}\text{Cf}$] the corresponding GCM and ATDHFB t_{SF} values are depicted in panels (a) and (b) [(c) and (d)] of Fig. 4, as functions of

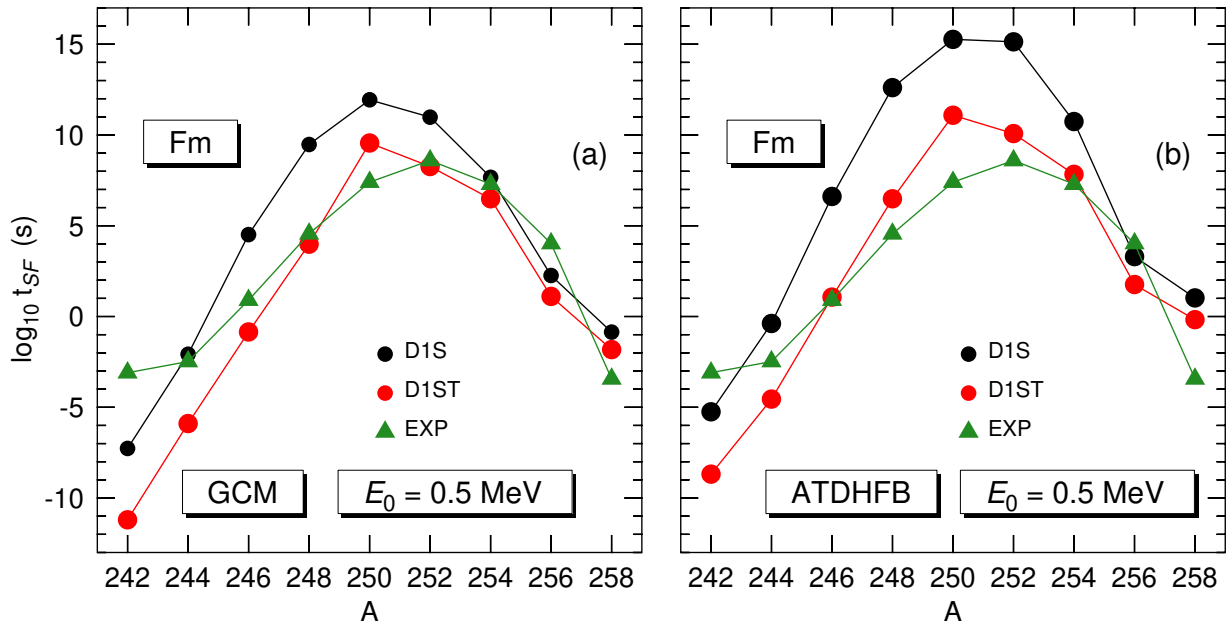


FIG. 5. (Color online) The spontaneous fission half-lives t_{SF} , predicted for the nuclei $^{242-258}\text{Fm}$, within the GCM and ATDHFB schemes, are depicted in panels (a) and (b) as functions of the mass number. Results have been obtained with the parametrizations D1S and D1ST of the Gogny-EDF and $E_0 = 0.5 \text{ MeV}$. The available experimental values, taken from Ref. [74], are included in the plots.

the mass number. The available experimental lifetimes [74] are also included in the panels. The results shown in the figure, have been obtained with $E_0 = 0.5 \text{ MeV}$ [7]. However, we have checked that other values of the parameter E_0 -for example, 1.0 MeV [7] and/or the value obtained from the curvature around the absolute minimum of the path and the collective quadrupole inertia [10]- do not alter qualitatively any of the conclusions of this work.

It is satisfying to observe from panels (a) and (c) of Fig. 4 that, for $^{240-250}\text{Cm}$ and $^{240-250}\text{Cf}$, the t_{SF} values predicted with both the D1S and D1ST Gogny-EDFs within the GCM scheme, reproduce reasonably well the observed experimental trend as a function of the mass number. In the case of $^{240-244}\text{Cm}$, the spontaneous fission half-lives obtained with the parametrization D1ST are smaller than the ones obtained with the standard parameter set D1S, while for larger mass numbers the former provides larger values than the latter. This behavior can be easily understood by taking into consideration first, that the inertias are very similar in the two cases and therefore their variations do not lead to substantial changes in the lifetimes. Second, but not least, the impact of the tensor term in the structure of the fission paths: for $^{240-244}\text{Cm}$, the first barrier is lower than the one obtained with D1S and the remaining of the collective potential looks rather similar. However, for heavier Cm isotopes, the much gentler decline of the path in the calculation with the tensor term gives an additional contribution to the action in the region $Q_{20} > 80b$.

On the other hand, for the considered Californium iso-

topes the D1ST Gogny-EDF always provides the smallest t_{SF} values as a consequence of the lower inner barrier heights and a similar decline of the fission path at large deformation. As can be seen from panels (b) and (d) similar features are observed for the spontaneous fission half-lives predicted within the ATDHFB scheme. This corroborates the robustness of the predicted D1S and D1ST trends with respect to the (GCM and/or ATDHFB) scheme employed in the calculations. Regardless of the EDF employed in the calculations, the ATDHFB t_{SF} values are always larger than the corresponding GCM lifetimes as a consequence of the larger ATDHFB inertias.

In order to further examine the predictive power of the D1ST parametrization, we have extended the calculations to $^{242-258}\text{Fm}$. The t_{SF} values, obtained for those Fermium isotopes, within the GCM and ATDHFB schemes, are depicted as functions of the mass number in panels (a) and (b) of Fig. 5. Calculations have been carried out with $E_0 = 0.5 \text{ MeV}$. The experimental belt-shaped dependence of the spontaneous fission half-lives, as functions of the mass number, is well reproduced by the D1S and D1ST Gogny-EDFs. With both parameter sets, the largest t_{SF} value is predicted two mass units earlier ($A=250$) than in the experiment. As in the Cm and Cf nuclei discussed before, the ATDHFB t_{SF} values are always larger than the GCM ones as a consequence of the larger inertias in the former case. Moreover, as with the larger Cf isotopes, for $^{242-258}\text{Fm}$ the parametrization D1ST provides smaller spontaneous fission half-lives. The explanation is similar to the one offered for the Cf

isotopes: the first fission barrier is lower with the tensor interaction and the gentler decline for large deformation observed in this case is not enough as to push the collective potential above $E_{min} + E_0$ and give a contribution to the action.

From the results discuss in this section, we conclude that the D1ST Gogny-EDF, including tensor contributions perturbatively [62–66], represents a reasonable starting point to describe spontaneous fission and related properties in heavy and low- Z superheavy nuclei.

IV. SUMMARY AND CONCLUSIONS

In this paper the impact on fission properties of a perturbative tensor term, added to the traditional Gogny D1S force, has been analyzed. Fission barrier heights and spontaneous fission half-lives are used as benchmark quantities. We observe that the tensor component of the force tends to push the position of maxima and minima of the collective potential to larger values of the quadrupole moment. The first fission barrier height is reduced by a couple of MeV as compared to the calculation without tensor. This is also true, but to a lesser extent, for the second barrier height. Additionally, the decline of the fission path beyond the second fission barrier is gentler when the tensor component is included. In the present approach, the tensor contribution to the pairing field is neglected and therefore the inclusion of the tensor has lit-

tle impact on the collective inertias. The combination of the three above mentioned effects: similar collective inertias, lower barrier heights and gentler decline of the collective potential make the spontaneous fission half-lives shorter in most of the cases when the tensor contribution is included. However, there are exceptions as the lower barrier heights and the gentler decline of the path are competing effects. From the results obtained in the Cm, Cf and Fm isotopic chains we conclude that the perturbative tensor term introduced has a non-negligible impact in fission dynamics and should be included in the calculations. Within this context, for example, the impact of the tensor pairing on the size of collective inertias, the role of triaxiality as well as the impact of tensor contributions in LA computations of spontaneous fission half-lives still deserve a detailed study. Work along these lines is in progress and will be reported in future publications.

ACKNOWLEDGMENTS

The work of LMR is supported by Spanish Agencia Estatal de Investigacion (AEI) of the Ministry of Science and Innovation under Grant No. PID2021-127890NB-I00. The work of R. Rodríguez-Guzmán was partially supported through the grant PID2022-136228NB-C22 funded by MCIN/AEI/10.13039/501100011033/FEDER, UE and "ERDF A way of making Europe".

-
- [1] O. Hahn and F. Strassmann, *Naturwissenschaften* **27**, 11 (1939).
 - [2] L. Meitner and O.R. Frisch, *Nature* **143**, 239 (1939).
 - [3] N. Bohr and J.A. Wheeler, *Phys. Rev.* **56**, 426 (1939).
 - [4] M. Bender *et al.*, *Journal of Physics G: Nuclear and Particle Physics* **47**, 113002 (2020).
 - [5] N. Schunck and L. M. Robledo, *Rep. Prog. Phys.* **79** 116301 (2016).
 - [6] P. Ring and P. Schuck, *The Nuclear Many-Body Problem* (Springer, Berlin, 1980).
 - [7] R. Rodríguez-Guzmán and L.M. Robledo, *Phys. Rev. C* **89**, 054310 (2014).
 - [8] R. Rodríguez-Guzmán, Y. M. Humadi and L. M. Robledo, *Eur. Phys. J. A* **56**, 43 (2020).
 - [9] R. Rodríguez-Guzmán and L. M. Robledo, *Eur. Phys. J. A* **50**, 142 (2014).
 - [10] R. Rodríguez-Guzmán and L. M. Robledo, *Eur. Phys. J. A* **52**, 12 (2016).
 - [11] H. Goutte, J. F. Berger, P. Casoli and D. Gogny, *Phys. Rev. C* **71**, 024316 (2005).
 - [12] D. Regnier, N. Dubray, N. Schunck and M. Verrière, *Phys. Rev. C* **93**, 054611 (2016).
 - [13] A. Zdeb, A. Dobrowolski and M. Warda, *Phys. Rev. C* **95**, 054608 (2017).
 - [14] J. F. Berger, M. Girod, and D. Gogny, *Nucl. Phys. A* **428**, 23c (1984).
 - [15] J.-P. Delaroche, M. Girod, H. Goutte and J. Libert, *Nucl. Phys. A* **771**, 103 (2006).
 - [16] N. Dubray, H. Goutte and J.-P. Delaroche, *Phys. Rev. C* **77**, 014310 (2008).
 - [17] W. Younes and D. Gogny, *Phys. Rev. C* **80**, 054313 (2009).
 - [18] M. Warda, J. L. Egido, L.M. Robledo and K. Pomorski, *Phys. Rev. C* **66**, 014310 (2002).
 - [19] M. Warda and J.L. Egido, *Phys. Rev. C* **86**, 014322 (2012).
 - [20] R. Rodríguez-Guzmán and L. M. Robledo, *Eur. Phys. J. A* **52**, 348 (2016).
 - [21] R. Rodríguez-Guzmán and L. M. Robledo, *Eur. Phys. J. A* **53**, 245 (2017).
 - [22] N. Nikolov, N. Schunck, W. Nazarewicz, M. Bender and J. Pei, *Phys. Rev. C* **83**, 034305 (2011).
 - [23] J.D. McDonnell, W. Nazarewicz and J.A. Sheikh, *Phys. Rev. C* **87**, 054327 (2013).
 - [24] J. Erler, K. Langanke, H.P. Loens, G. Martínez-Pinedo and P.-G. Reinhard, *Phys. Rev. C* **85**, 025802 (2012).
 - [25] A. Staszczak, A. Baran, W. Nazarewicz, *Phys. Rev. C* **87**, 024320 (2013).
 - [26] A. Baran, K. Pomorski, A. Lukasiak and A. Sobczewski, *Nucl. Phys. A* **361**, 83 (1981).
 - [27] M. Baldo, L.M. Robledo, P. Schuck and X. Viñas, *Phys. Rev. C* **87**, 064305 (2013).
 - [28] S. A. Giuliani and L.M Robledo, *Phys. Rev. C* **88**, 054325 (2013).
 - [29] Samuel A. Giuliani, Gabriel Martnez-Pinedo, and Luis M. Robledo *Phys. Rev. C* **97**, 034323 (2018).

- [30] H. Abusara, A.V. Afanasjev and P. Ring, Phys. Rev. C **82**, 044303 (2010).
- [31] H. Abusara, A.V. Afanasjev and P. Ring, Phys. Rev. C **85**, 024314 (2012).
- [32] B.-N. Lu, E.-G. Zhao and S.-G. Zhou, Phys. Rev. C **85**, 011301 (2012).
- [33] S. Karatzikos, A. V. Afanasjev, G. A. Lalazissis and P. Ring, Phys. Lett. B **689**, 72 (2010).
- [34] M. Bender, K. Rutz, P.-G. Reinhard, J.A. Maruhn and W. Greiner, Phys. Rev. C **58**, 2126 (1998).
- [35] Z. Shi, A. V. Afanasjev, Z. P. Li and J. Meng, Phys. Rev. C **99**, 064316 (2019).
- [36] A. Taninah, S. E. Agbemava and A. V. Afanasjev, Phys. Rev. C **102**, 054330 (2020).
- [37] R. Rodríguez-Guzmán and L. M. Robledo, Phys. Rev. C **107**, 044307 (2023).
- [38] J. Sadhukhan, K. Mazurek, A. Baran, J. Dobaczewski, W. Nazarewicz and J. A. Sheikh, Phys. Rev. C **88**, 064314 (2013).
- [39] S.A. Giuliani, L. M. Robledo and R. Rodríguez-Guzmán, Phys. Rev. C **90**, 054311 (2014).
- [40] R. Rodríguez-Guzmán and L. M. Robledo, Phys. Rev. C **98**, 034308 (2018).
- [41] K. Pomorski. Int. J. of Mod. Phys. E **16**, 237 (2007).
- [42] A. Staszczak, S. Pilat and K. Pomorski, Nucl. Phys. A **504**, 589 (1989).
- [43] J. Sadhukhan, W. Nazarewicz and N. Schunck, Phys. Rev. C **93**, 011304 (2016).
- [44] J. Sadhukhan, J. Dobaczewski, W. Nazarewicz, J. A. Sheikh and A. Baran, Phys. Rev. C **90**, 061304(R) (2014).
- [45] J. Zhao, B. -N. Lu, T. Niksic, D. Vretenar and S. -G. Zhou, Phys. Rev. C **93**, 044315 (2016).
- [46] Dechargé and D. Gogny, Phys. Rev. C **21**, 1568 (1980).
- [47] L. M. Robledo, T. R. Rodriguez and R. Rodríguez-Guzmán, J. Phys. G: Nucl. Part. Phys. **46**, 013001 (2019).
- [48] J.D. McDonnell, W. Nazarewicz and J.A. Sheikh, Phys. Rev. C **87**, 054327 (2013).
- [49] F. Chappert, M. Girod, and S. Hilaire, Phys. Lett. B **668**, 420 (2008).
- [50] S. Goriely, S. Hilaire, M. Girod and S. Péru, Phys. Rev. Lett. **102**, 242501 (2009).
- [51] R. Rodríguez-Guzmán, L.M. Robledo and P. Sarriguren, Phys. Rev. C **86**, 034336 (2012).
- [52] R. Rodríguez-Guzmán, L.M. Robledo, P. Sarriguren and J. E. García-Ramos, Phys. Rev. C **81**, 024310 (2010).
- [53] L.M. Robledo, R. Rodríguez-Guzmán, and P. Sarriguren, J. Phys. G: Nucl. Part. Phys. **36**, 115104 (2009).
- [54] L.M. Robledo and R. Rodríguez-Guzmán, J. Phys. G: Nucl. Part. Phys. **39**, 105103 (2012).
- [55] R. Rodríguez-Guzmán, P. Sarriguren, and L.M. Robledo, Phys. Rev. C **82**, 061302(R) (2010).
- [56] R. Rodríguez-Guzmán, P. Sarriguren, and L.M. Robledo, Phys. Rev. C **83**, 044307 (2011).
- [57] R. Rodríguez-Guzmán and L.M. Robledo, Phys. Rev. C **108**, 024301 (2023).
- [58] R. Rodríguez-Guzmán and L.M. Robledo, Phys. Rev. C **103**, 044301 (2021).
- [59] T. Lesinski, M. Bender, K. Bennaceur, T. Duguet and J. Meyer, Phys. Rev. C **76**, 014312 (2007).
- [60] M. Bender, K. Bennaceur, T. Duguet, P.-H. Heenen, T. Lesinski, and J. Meyer, Phys. Rev. C **80**, 064302 (2009).
- [61] T. Otsuka, T. Matsuo and D. Abe, Phys. Rev. Lett. **97**, 162501 (2006).
- [62] M. Anguiano, G. C6, V. De Donno and A. M. Lallena, Phys. Rev. C **83**, 064306 (2011).
- [63] M. Anguiano, M. Grasso, G. C6, V. De Donno and A. M. Lallena, Phys. Rev. C **86**, 054302 (2012).
- [64] M. Grasso and M. Anguiano, Phys. Rev. C **88**, 054328 (2013).
- [65] M. Anguiano, A. M. Lallena, G. C6, V. De Donno, M. Grasso and R. N. Bernard, Eur. Phys. J. A **52**, 183 (2016).
- [66] R. N. Bernard and M. Anguiano, Nucl. Phys. A **953**, 32 (2016).
- [67] D. Gogny, P. Pires, and R. de Tourreil, Phys. Lett. B **32**, 591 (1970).
- [68] F. Chappert, N. Pillet, M. Girod, and J.-F. Berger, Phys. Rev. C **91**, 034312 (2015).
- [69] N. Pillet and S. Hilaire, Eur. Phys. J. A **53**, 193 (2017).
- [70] R. N. Bernard, N. Pillet, L. M. Robledo and M. Anguiano, Phys. Rev. C **101**, 044615 (2020).
- [71] A. Chatillon *et al.*, Phys. Rev. C **99**, 054628 (2019).
- [72] J.-F. Martinet *et al.*, Eur. Phys. J A **51**, 174 (2015); E. Pellereau *et al.*, Phys. Rev. C **95**, 054603 (2017).
- [73] A. Chatillon *et al.*, Phys Rev Lett **124**, 202502 (2020); A. Chatillon *et al.*, Phys. Rev. C **106**, 024618 (2022).
- [74] N. E. Holden and D. C. Hoffman, Pure Appl. Chem. **72**, 1525 (2000).
- [75] L.M. Robledo and G. F. Berstch, Phys. Rev. C **84**, 014312 (2011).
- [76] C. Titin-Schnaider and Ph. Quentin, Phys. Lett. B **49**, 213 (1974).
- [77] M. Brack, J. Damgaard, A.S. Jensen, H.C. Pauli, V.M. Strutinsky and C.Y. Wong, Rev. Mod. Phys. **44**, 320 (1972).
- [78] M. Girod and B. Grammaticos, Nucl. Phys. A **330**, 40 (1979).
- [79] M.J. Giannoni and P. Quentin, Phys. Rev. C **21**, 2060 (1980); Phys. Rev. C **21**, 2076 (1980).
- [80] J. Libert, M. Girod and J.P. Delaroche, Phys. Rev. C **60**, 054301 (1999).
- [81] J.L. Egido and L.M. Robledo, Lectures Notes in Physics **641**, 269 (2004).
- [82] R. Rodríguez-Guzmán, J.L. Egido and L.M. Robledo, Phys. Lett. B **474**, 15 (2000); Phys. Rev. C **62**, 054308 (2000).
- [83] R. Rodríguez-Guzmán, J.L. Egido and L.M. Robledo, Nucl. Phys. A **709**, 201 (2002).
- [84] J.F. Berstch and H. Flocard, Phys. Rev. C **43**, 2200 (1991).
- [85] B. Singh, R. Zywina and R. Firestone, Nucl. Data Sheets **97**, 241 (2002).
- [86] R. Capote *et al.*, Nucl. Data Sheets **110**, 3107 (2009).
- [87] G.F. Bertsch, W. Loveland, W. Nazarewicz, and P. Talou, J. Phys. G Nucl. Part. Phys. **42**, 077001 (2015).